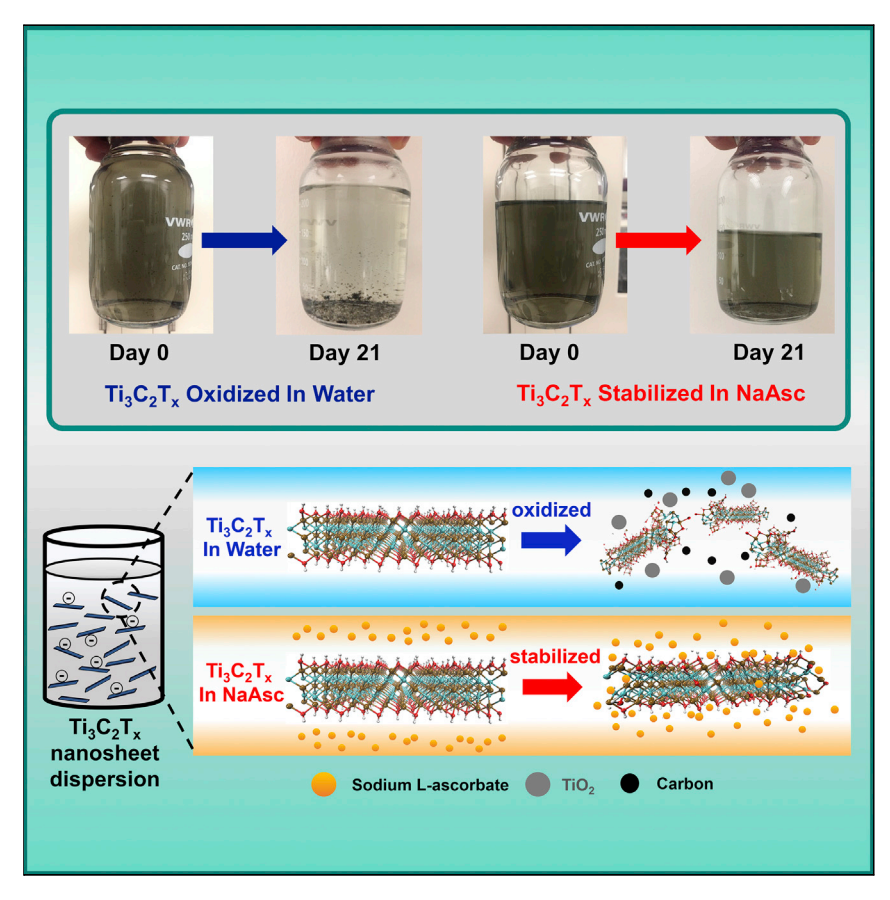
Matter Cell Press

Article

Antioxidants Unlock Shelf-Stable $Ti_3C_2T_x$ (MXene) Nanosheet Dispersions



MXenes are prone to oxidize and degrade quickly in a matter of days. Here, the use of antioxidants, such as sodium L-ascorbate, is demonstrated as an effective approach to arrest the oxidation of colloidal and dehydrated $\text{Ti}_3\text{C}_2\text{T}_x$ MXene nanosheets. The success of the method is evident as the $\text{Ti}_3\text{C}_2\text{T}_x$ nanosheets maintain their composition, morphology, electrical conductivity, and colloidal stability. This method addresses the most pressing challenge in the field of MXene engineering.

Xiaofei Zhao, Aniruddh Vashisth, Evan Prehn, ..., Jodie L. Lutkenhaus, Miladin Radovic, Micah J. Green

micah.green@tamu.edu

HIGHLIGHTS

Shelf-stable MXenes are enabled by introducing antioxidants

Structures and properties of ${\rm Ti}_3{\rm C}_2{\rm T}_x$ MXene are stabilized by sodium L-ascorbate

Antioxidant protects MXene by restricting water accessing the reactive sites



Zhao et al., Matter 1, 513–526 August 7, 2019 © 2019 Elsevier Inc. https://doi.org/10.1016/j.matt.2019.05.020





Article

Antioxidants Unlock Shelf-Stable Ti₃C₂T_x (MXene) Nanosheet Dispersions

Xiaofei Zhao,¹ Aniruddh Vashisth,² Evan Prehn,³ Wanmei Sun,¹ Smit A. Shah,¹ Touseef Habib,¹ Yexiao Chen,³ Zeyi Tan,³ Jodie L. Lutkenhaus,^{1,3} Miladin Radovic,³ and Micah J. Green^{1,3,4,*}

SUMMARY

Although MXene nanosheets have attracted significant scientific and industrial attention, these materials are highly susceptible to oxidation, which leads to their chemical degradation and loss of functional properties in a matter of days. Here we demonstrate an effective method to prevent the oxidation of colloidal $Ti_3C_2T_x$ MXene nanosheets by using sodium L-ascorbate as an antioxidant. The success of the method is evident in the stable morphology, structure, and colloidal stability of $Ti_3C_2T_x$. Even in the presence of water and oxygen, the electrical conductivity of $Ti_3C_2T_x$ nanosheets treated with sodium L-ascorbate was orders of magnitude higher as compared with untreated ones after 21 days. This resistance to oxidation also persists in the dried state. We propose that the sodium L-ascorbate protects the edges of the nanosheets, restricting water molecules from otherwise reactive sites; this is supported by molecular dynamics simulations that show association of the ascorbate anion with the nanosheet edge.

INTRODUCTION

MXenes are a family of two-dimensional (2D) transition metal carbides, carbonitrides, and nitrides; in recent times there has been an avalanche of research studies and material applications focused on MXenes because of their fascinating combination of physical and electrochemical properties; ¹ prior studies have highlighted MXenes' hydrophilicity, excellent electrical and thermal conductivities, ease of processability, and in-plane stiffness. ^{2,3} These materials hold promise for a wide range of applications in batteries, supercapacitors, electronic sensors, electromagnetic interference shielding, and electrocatalysts. ^{4–10} Even though MXenes have been praised for their physical and electrochemical properties, one particular problem has plagued both the science and applications of these materials: most known MXenes are prone to oxidation, resulting in the loss of both their nanosheet structure and functional properties.

MXenes are generally described as 2D materials with the chemical formula of $M_{n+1}X_nT_x$, where M represents an early transition metal element such as titanium (Ti), vanadium (V), or niobium (Nb), X is carbon and/or nitrogen, T refers to one or multiple terminal groups, n ranges from 1 to 3, and x reflects the number of terminal groups. ^{10,11} MXenes are typically synthesized from a parent MAX phase bearing an atomically layered crystal structure, ¹² in which $M_{n+1}X_n$ layers are interleaved by a layer of the A element (from group 13 or 14), such as aluminum (Al), tin (Sn), or silicon (Si). Layered MXene "clay" can be derived by selective etching and removal of the A layer from the parent MAX phase. ^{13,14} Furthermore, this clay may be intercalated, delaminated, and exfoliated to yield individual MXene nanosheets.

Progress and Potential

MXenes such as Ti₃C₂T_x are fascinating two-dimensional nanomaterials with an attractive combination of functional properties suitable for applications such as batteries, supercapacitors, and sensors. However, fabrication of devices and functional coatings based on MXenes remains challenging as they oxidize and degrade quickly in water. We demonstrate an effective approach to arrest the oxidation of colloidal Ti₃C₂T_x MXene nanosheets by introducing antioxidants such as sodium L-ascorbate. The success of the method is evident as the Ti₃C₂T_x nanosheets maintain composition, morphology, electrical conductivity, and colloidal stability. This study reveals that the resistance to oxidation persists in the dehydrated MXenes as well. We also show that other antioxidants may be similarly effective. These findings have the potential to be generalized to protect other types of MXenes and solve the most pressing challenge in the field of MXene engineering.



Matter Cell²ress

This study focuses on $Ti_3C_2T_x$ nanosheets, one of the most studied members in the MXene family. These are typically derived by the wet acid etching of parent Ti_3AlC_2 to produce $Ti_3C_2T_x$ nanosheets in which the terminal groups include hydroxyl (-OH), oxygen (-O), fluoride (-F), and chloride (-Cl), depending on the acid in question. ^{15–17} These polar terminal groups result in strong hydrophilicity and electronegativity, which allow them to be dispersed in water and form a suspension. In addition, the types and distribution of terminal groups can have a strong impact on the properties, stability, and functionality of MXenes. ¹⁷

Unfortunately, Ti₃C₂T_x tends to oxidize and degrade rapidly over the course of days when exposed to air and/or water, leading to the disassembly of the layered, 2D structure and formation of titanium dioxide (TiO₂) and carbon (C). 18-20 This degradation has been observed by transmission electron microscopy and even by direct observation of color changes of nanosheet dispersions from a black/dark green color to a cloudy white/brownish color.²¹ Several prior studies have explored the issue of MXene oxidation. Our group recently observed that the oxidation rate varies widely depending on the surrounding media; specifically, the oxidation rates were substantially higher in aqueous phases compared with organic solvents, air, and solid media.²² Maleski et al. also reported evidence showing that organic solvents can mitigate or slow MXene degradation compared with water.²³ Reactive molecular dynamics simulations suggest that the $Ti_3C_2T_x$ oxidation rate depends on both temperature and available oxidant concentration.²⁴ Prior studies have also indicated that the oxidation starts at the MXene edges and defects. The asformed metal oxide nanocrystals can then develop throughout the MXene flake by nucleation and growth. 20,25 It is noteworthy that MXenes with multilayered/ stacked structures are less prone to oxidation than individual nanosheets due to the stacked structure's lower surface-to-volume ratio; even so, Mashtalir et al. and Habib et al. observed oxidation of multilayer stacks over the course of several days indicated by the rapid appearance of titanium dioxide and the dramatic decrease in electrical conductivity. 19,22 In the individual nanosheet form, MXenes typically show better electrical performance, colloidal stability, and processability but lower oxidation stability compared with multilayered MXene clay. 22,26 Zhang et al. studied the degradation of delaminated Ti₃C₂T_x colloidal solutions stored in open vials and concluded that Ti₃C₂T_x MXenes can severely oxidize and degrade after 15 days.²⁰ Thus, strategies to preserve MXene nanosheets and avoid oxidation are critical for both MXene nanosheets in dispersions and stacked MXenes in clays or buckypaper films.

Only a handful of studies have suggested strategies for mitigating ${\rm Ti_3C_2T_x}$ oxidation, mostly centering on the restriction of oxygen exposure at low temperature. Anasori et al. mentioned that MXenes are more stable in oxygen-free degassed water or in dry air, and that light exposure can accelerate oxidation. The accelerate oxidation still occurs at a specific proposed the storage of degassed ${\rm Ti_3C_2T_x}$ aqueous dispersions in hermetic argon-filled containers at 5°C. However, they reported that oxidation still occurs at those conditions, but at slower rate. It is noteworthy that oxygen solubility is quite low (around 8 mg/L at 25°C), so it is difficult to attribute oxidation solely to dissolved oxygen, and water itself is likely to play a major role in oxidation; 20,22,27 we explore this possibility in further detail below. Other techniques to slow or prevent oxidation include freezing and freeze-drying MXenes under vacuum. We at al. proposed a carbon nanoplating technique to modify ${\rm Ti_3C_2}$ MXene surface for inhibiting oxygen diffusion. Despite these efforts, effective techniques to eliminate or restrict the oxidation of MXene nanosheets remain elusive, particularly in the dispersed aqueous state.

¹Artie McFerrin Department of Chemical Engineering, Texas A&M University, College Station, TX 77843, USA

²Department of Aerospace Engineering, Texas A&M University, College Station, TX 77843, USA

³Department of Material Science & Engineering, Texas A&M University, College Station, TX 77843, USA

⁴Lead Contact

^{*}Correspondence: micah.green@tamu.edu https://doi.org/10.1016/j.matt.2019.05.020

Matter Cell²ress

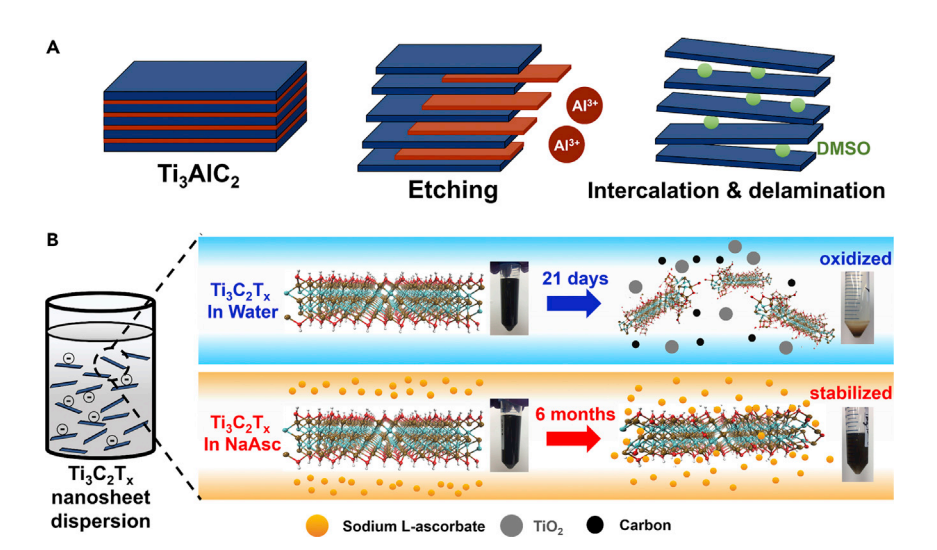


Figure 1. Schematics of Shelf-Stable Ti₃C₂T_x Nanosheet Dispersion Enabled by the Antioxidant Sodium L-Ascorbate

(A) Schematic representation of $Ti_3C_2T_x$ nanosheet synthesis: Aluminum (Al) layer is removed from the parent Ti_3AlC_2 by acid etching, and the resulting multilayer MXene clay was intercalated by DMSO and delaminated by sonication.

(B) Shelf-stable $Ti_3C_2T_x$ nanosheets stabilized by sodium L-ascorbate (NaAsc). The $Ti_3C_2T_x$ MXene nanosheets were stored both in deionized water and NaAsc solution. Without antioxidant, the $Ti_3C_2T_x$ oxidizes and degrades to form TiO_2 and carbon. Sodium L-ascorbate shields the nanosheet from being severely oxidized. The $Ti_3C_2T_x$ retained its as-prepared appearance after 6 months; however, the appearance of colloidal $Ti_3C_2T_x$ nanosheets stored in water was completely changed.

Here, we hypothesize that an antioxidant added to the aqueous MXene dispersion will preserve $Ti_3C_2T_x$ nanosheets by restricting oxidation and thus extending their shelf life (shown schematically in Figure 1). To this end, we use sodium L-ascorbate (NaAsc), which is widely available and has been used in food and pharmaceutical industries as a preservative or antioxidant. We show that the chemical composition, 2D layered structure, and colloidal stability of $Ti_3C_2T_x$ nanosheets are retained even after 21 days when stored in NaAsc-stabilized dispersions, in stark contrast to those stored for the same duration in $Ti_3C_2T_x$ /water dispersions. Reactive molecular dynamics (ReaxFF) simulations are also used to probe the mechanism of these interactions between $Ti_3C_2T_x$ nanosheets and NaAsc that led to the stabilization of $Ti_3C_2T_x$ nanosheets.

RESULTS AND DISCUSSION

Sodium L-Ascorbate Promotes MXene Stability against Oxidation and Aggregation

Colloidal $Ti_3C_2T_x$ nanosheet dispersions were diluted with a premixed aqueous solution of NaAsc, which acts as an antioxidant and ensures a reducing environment, to obtain a concentration of 6.1 \times 10⁻³ mg/mL MXene and 1 mg/mL NaAsc. The NaAsc-stabilized dispersions were stored for 21 days in closed bottles at ambient temperature. No degassing was practiced before or during the storage, such that the MXene colloidal solution was in contact with the bottle's headspace (air). Control dispersions were made by diluting $Ti_3C_2T_x$ MXene colloid with deionized water to the same final concentration and stored under identical conditions for 21 days.

X-ray diffraction (XRD) patterns of (i) dried $Ti_3C_2T_x$ nanosheets previously stored in 1 mg/mL NaAsc solution after 21 days were compared with those of (ii) as-prepared $Ti_3C_2T_x$ nanosheets, (iii) $Ti_3C_2T_x$ nanosheets previously kept in deionized water, and



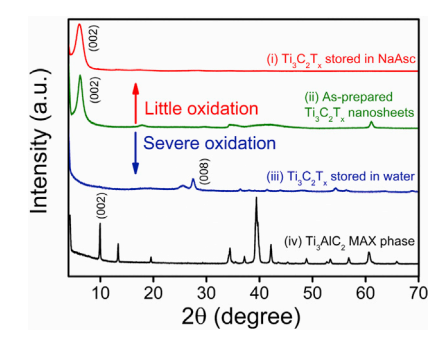


Figure 2. Crystalline Structural Properties of Ti₃AlC₂ and Ti₃C₂T_x Characterized Using X-Ray Diffraction

XRD patterns for $Ti_3C_2T_x$ nanosheets stored for 21 days in deionized water (i) with and (iii) without NaAsc, exhibiting little and severe oxidation, respectively, as compared with (ii) as-prepared $Ti_3C_2T_x$ nanosheets. All nanosheets were obtained after etching, intercalation, and delamination. (iv) XRD pattern for the Ti_3AlC_2 MAX phase. Samples used for XRD were prepared by vacuum filtration followed by vacuum drying at 40° C for 12 h.

(iv) the parent Ti_3AlC_2 MAX phase (Figure 2). After etching, intercalation, and further delamination, the pronounced (002) peak shifts from a 2θ angle of 9.7° that is typical for the parent MAX phase to a lower 2θ angle of around 6.5°, which is typical for $Ti_3C_2T_x$ nanosheets. ²⁹ The (002) peak tends to broaden gradually in the processing stages, which most likely suggests an increased d-spacing and decreased thickness of $Ti_3C_2T_x$ layers. ^{29,30} After being stored in NaAsc solution for 21 days, the colloidal $Ti_3C_2T_x$ nanosheets retained their pronounced (002) peak at a 2θ angle of around 6.5°. However, the (002) peak disappeared completely from the XRD spectrum for $Ti_3C_2T_x$ stored in deionized water, indicating the total oxidation of crystalline MXene to an amorphous structure. Collectively, these XRD results suggest that the crystalline structure of $Ti_3C_2T_x$ nanosheets can be effectively retained by introducing an antioxidant.

To detect changes in colloidal stability caused by oxidation, we measured the hydrodynamic size distributions (shown in Figure 3A) of ${\rm Ti_3C_2T_x}$ dispersions using dynamic light scattering (DLS). After 6 days, the average size of the material dispersed in water increased dramatically due to nanosheet agglomeration (corroborated by ζ potential measurements below). At around day 15, the average hydrodynamic diameter reached a maximum value of nearly 2,200 nm. However, after 15 days the hydrodynamic diameter declined; this is likely associated with further oxidation and degradation to ${\rm TiO_2}$. In contrast, samples dispersed in the NaAsc solution exhibited a much more constant size distribution over time. The average hydrodynamic diameter based on intensity was found to be invariant at around 500 nm, which suggests that introducing NaAsc is an effective way to retain the lateral size of ${\rm Ti_3C_2T_x}$ nanosheets, thus limiting oxidation and maintaining colloidal stability.

The colloidal stability of $Ti_3C_2T_x$ dispersions was further examined by characterizing ζ potential over time (Figure 3B). The surface of a $Ti_3C_2T_x$ nanosheet is negatively charged due to the terminal groups (i.e., -OH, -O, -Cl, and -F). The change in ζ potential reflects a decrease in the amount of surface charge, which is caused by the oxidation of $Ti_3C_2T_x$ nanosheets. Nanosheets stored in NaAsc solution generally maintained a stable ζ potential (below -35 mV) during the 21-day storage. In contrast, a significant weakening of ζ potential was observed for nanosheets stored in deionized water even during the first day, which indicates a rapid loss of colloidal stability.

Matter Cell^Press

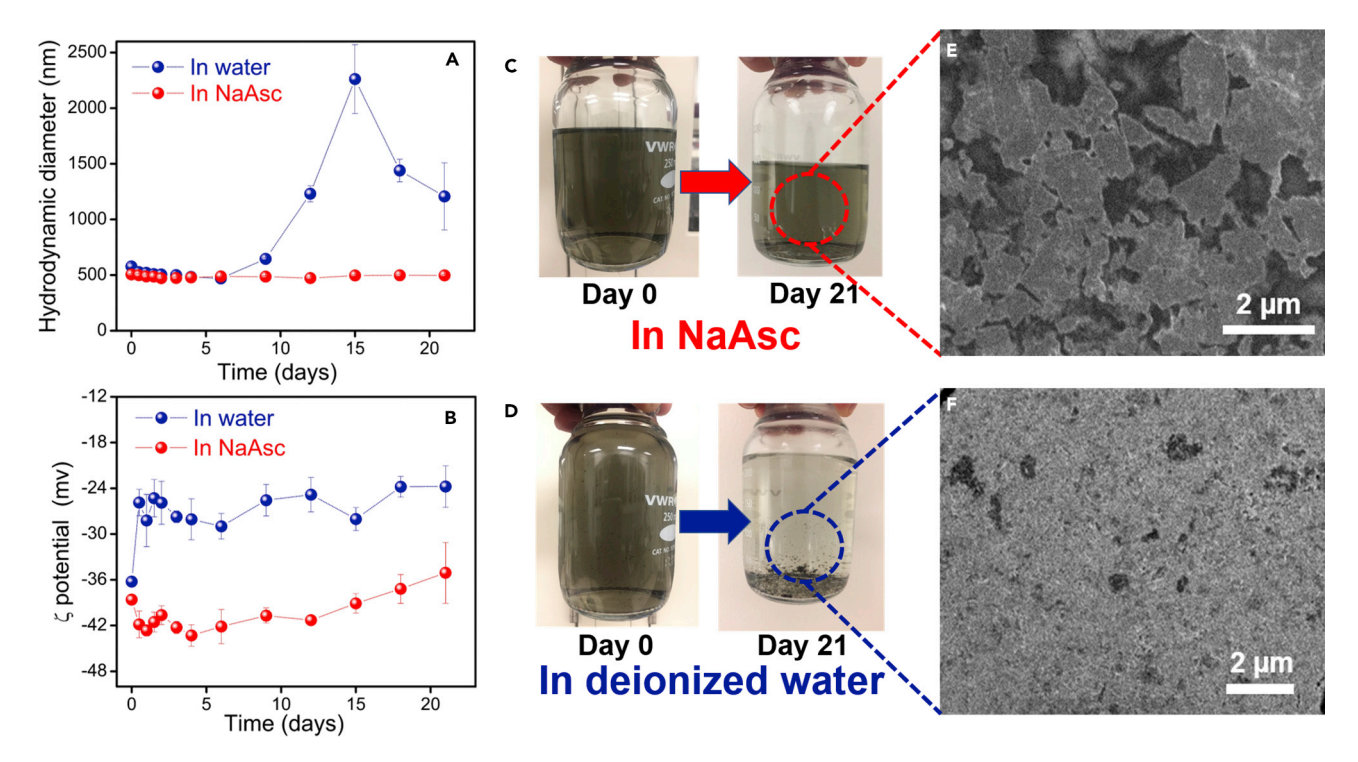


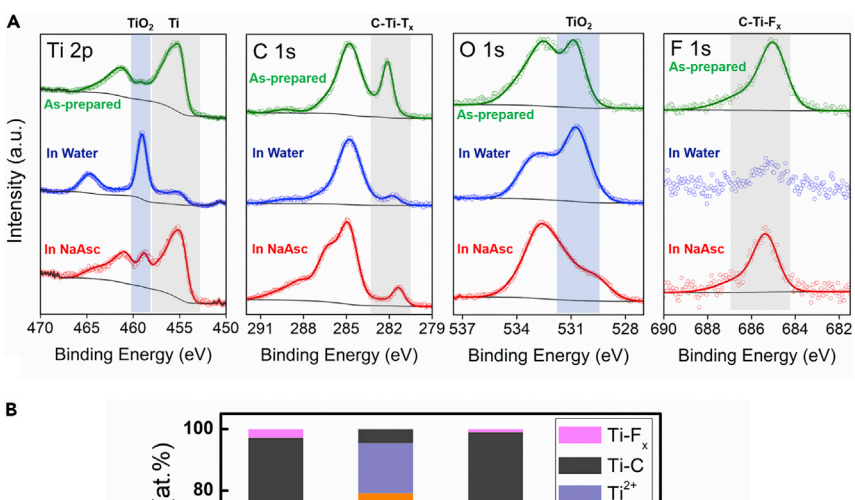
Figure 3. Colloidal Stability and Morphology of Shelf-Stable Ti₃C₂T_x Nanosheets

- (A) The average hydrodynamic diameter of $Ti_3C_2T_x$ nanosheets measured as a function of time for dispersions in deionized water and 1 mg/mL NaAsc solution.
- (B) Time evolution of ζ potential of Ti₃C₂T_x dispersions in deionized water and 1 mg/mL NaAsc solution (see also Figure S1).
- (C and D) Corresponding images of the dispersions at day 0 and day 21 in NaAsc (C) and deionized water (D)
- (E) Scanning electron microscopy (SEM) image of $Ti_3C_2T_x$ nanosheets after being stored in 1 mg/mL NaAsc solution for 21 days indicates that the nanosheets retain their morphology.
- (F) SEM image of drop-cast $Ti_3C_2T_x$ nanosheets after being stored in deionized water for 21 days shows an amorphous and dense structure.

The $Ti_3C_2T_x$ nanosheet dispersions stored in 1 mg/mL NaAsc solution and water after 21 days are compared in Figures 3C and 3D, respectively. In addition, aggregates were observed after only a few days in the water dispersion. When stored in deionized water without antioxidant, the $Ti_3C_2T_x$ MXene nanosheet dispersion shows a dramatic color change from day 0 to day 21: the dispersion became lighter on visual inspection as most $Ti_3C_2T_x$ nanosheets oxidized into TiO_2 and C. Visible precipitated clusters of $Ti_3C_2T_x$ MXene nanosheets were also observed during the storage. In contrast, the aqueous $Ti_3C_2T_x$ MXene nanosheet dispersion stored in NaAsc exhibited little color change or aggregation.

The effectiveness of NaAsc in protecting the MXene structure was analyzed by characterizing the final morphologies of the stored $Ti_3C_2T_x$ nanosheets using scanning electron microscopy. Figure 3E reveals that the morphology of the nanosheets was successfully retained for the materials preserved in NaAsc solution after 21 days. However, the $Ti_3C_2T_x$ previously stored in water exhibited an amorphous TiO_2 structure, displayed in Figure 3F. The typical nanosheet morphology could not be observed in this sample; instead, a clay-like paste was seen.

The chemical composition of $Ti_3C_2T_x$ nanosheets was characterized using X-ray photoelectron spectroscopy (XPS). The presences of titanium (Ti), carbon (C), oxygen (O), and fluorine (F) in as-prepared and stored $Ti_3C_2T_x$ were confirmed in the survey spectra (Figures S2–S4). High-resolution spectra of Ti 2p, C 1s, O 1s, and F 1s are



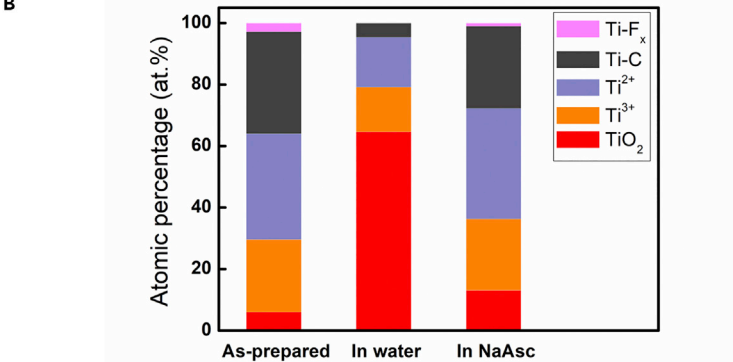


Figure 4. Chemical Composition of As-Prepared Ti₃C₂T_x Nanosheets and Nanosheets Stored after 21 Days

(A) XPS spectra of Ti 2p, C 1s, O 1s, and F 1s for as-prepared $Ti_3C_2T_x$ nanosheets, nanosheets stored in deionized water, and those stored in 1 mg/mL solution of NaAsc after 21 days. Deconvolutions and associated binding energy values are listed in Tables S1–S3. The Ti 2p spectra shows that the peak corresponding to TiO_2 increased in intensity and that the Ti peak greatly decreased in intensity for the nanosheets dispersed in water when compared with as-prepared MXenes and those stored in NaAsc. This shows that the chemical composition of $Ti_3C_2T_x$ nanosheets was largely retained when NaAsc was present.

(B) XPS peak fitting results for the Ti 2p region for $Ti_3C_2T_x$ MXenes. The atomic percentages of TiO_2 (Ti^{4+}), Ti^{3+} , Ti^{2+} , Ti^{-2} , and C-Ti- F_x obtained from the deconvoluted Ti 2p region for as-prepared and stored $Ti_3C_2T_x$ nanosheets in water and NaAsc solution are shown. $Ti_3C_2T_x$ stored in water shows the highest percentage of TiO_2 due to severe oxidation. Sodium L-ascorbate inhibits oxidation; the TiO_2 fraction remains relatively much less changed when compared with the sample stored in water.

displayed in Figure 4A. Ti 2p spectra were deconvoluted into Ti⁺ (Ti-C and Ti-F), Ti²⁺, Ti³⁺, and Ti⁴⁺ (TiO₂) (Figure S5). For both the as-prepared Ti₃C₂T_x and the Ti₃C₂T_x stored in NaAsc solution, the TiO₂ (Ti⁴⁺) comprises relatively low atomic fractions in the Ti 2p region (around 6.1 atom % and 13.1 atom %, respectively). However, for the sample stored in water for 21 days, the TiO₂ (Ti⁴⁺) comprises a much higher atomic fraction, around 64.6 atom % of the photoemission in Ti 2p region. This can be confirmed by the high-intensity peak around 459 eV, which is evidence of the severe oxidation of Ti₃C₂T_x MXene.

The XPS peaks of the Ti 2p region give important insights into the effect of NaAsc on the oxidation states of titanium within the $Ti_3C_2T_x$ nanosheets. The relative atomic compositions of Ti^{4+} , Ti^{3+} , Ti^{2+} , and Ti^+ species in aged aqueous $Ti_3C_2T_x$ dispersion (with and without antioxidant) are compared in Figure 4B. As expected, in the case of aging in water, we observe an increase in the relative composition of Ti species with higher oxidation states (i.e., Ti^{2+} and Ti^{3+} are oxidized to Ti^{4+} , and Ti^{4-} is oxidized to

Matter Cell²ress

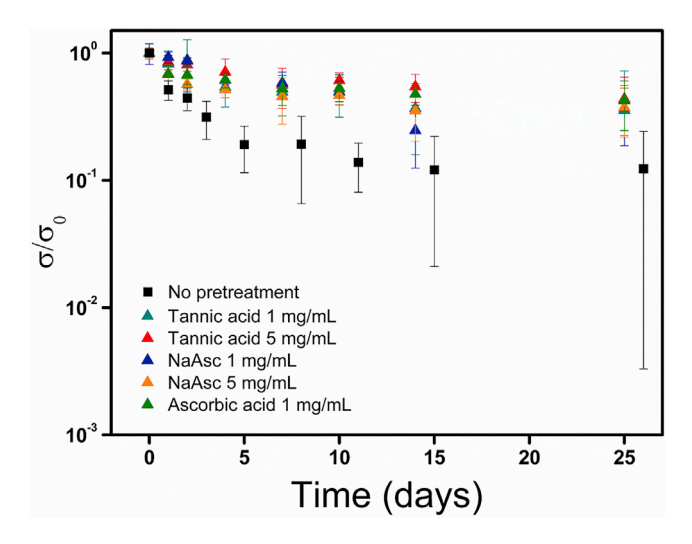


Figure 5. Normalized Conductivity Change over Time for Buckypaper Made from $Ti_3C_2T_x$ **Pretreated by Antioxidants**

Conductivity changes were measured for dried filtered films made from Ti₃C₂T_x nanosheets pretreated by various antioxidants. The drastic reduction of normalized electrical conductivity (σ/σ_0) due to oxidation was inhibited by the antioxidants. This acts as evidence that antioxidants in general prevent oxidation of $Ti_3C_2T_x$ nanosheets in the dried form. (σ is the real-time conductivity [S/m], σ_0 is the initial conductivity of as-prepared Ti₃C₂T_x film.)

Ti²⁺ and Ti³⁺). However, in the presence of NaAsc, the chemical state transition from Ti⁺ to Ti²⁺/Ti³⁺ was inhibited; the increase of Ti⁴⁺ with time was slow.

The electrical conductivity of the macroassembly of layered $Ti_3C_2T_x$ nanosheets can also be used as an indicator of the degree of oxidation.²² Table S4 displays the changes in the electrical conductivities of MXene filtered films made from the as-prepared (day 0) and stored (day 21) $Ti_3C_2T_x$ nanosheets in NaAsc solution and deionized water, respectively. The electrical conductivity for the MXene film comprised of as-prepared $Ti_3C_2T_x$ nanosheets (3.2 \pm 0.3 \times 10⁵ S/m) was consistent with prior studies.³⁰ After storage in deionized water, the filtered MXene film conductivity dropped below 10^{-6} S/m. In contrast, the film made from Ti₃C₂T_x stored in NaAsc solution retained an electrical conductivity of $5.7 \pm 0.5 \times 10^4$ S/m, with a decrease of less than one order of magnitude. The relative electrical conductivity stability is evidence that NaAsc protects the $Ti_3C_2T_x$ nanosheets from severe oxidation.

Oxidation Prevention for Dried Ti₃C₂T_x

Dried MXene nanosheets are also known to undergo oxidization when stored in ambient conditions.²² With this in mind, we tested whether antioxidant-treated MXenes would resist oxidation in the dry form as powders or films. We prepared vacuum-filtered Ti₃C₂T_x films that were made from colloidal nanosheet dispersions that had been pretreated with several antioxidants, including NaAsc, tannic acid, and ascorbic acid. Figure 5 shows that the decrease of normalized electrical conductivity (σ/σ_0) can be substantially slowed by the antioxidants introduced in the pretreatment steps; this indicates that the antioxidants alter oxidation chemistry not only in solution but also in the dried state. (The absolute electrical conductivity values can be found in Figure S6.) This technique can potentially make shelf-stable MXenes suitable for a variety of applications in the dry environment without substantial oxidation.

Matter Cell²ress

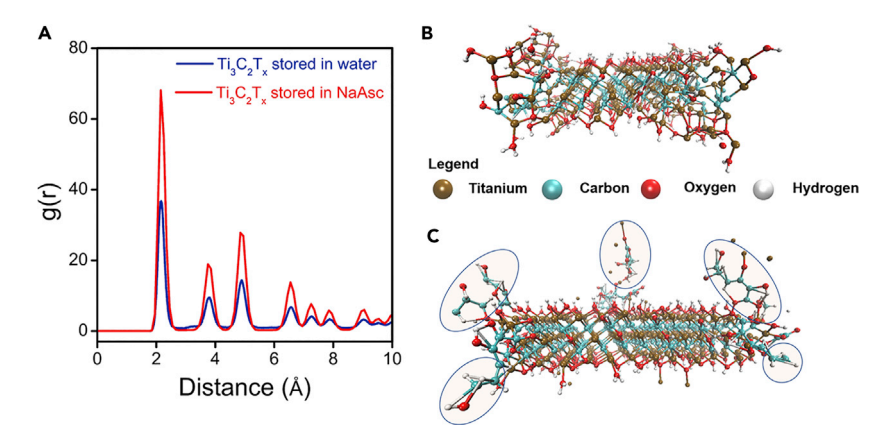


Figure 6. Reactive Molecular Dynamics Simulation of Shelf-Stable Ti₃C₂T_x MXenes

(A) The radial distribution functions of Ti-C bonds obtained by ReaxFF are shown for stored ${\rm Ti}_3{\rm C}_2{\rm T}_x$ nanosheets. A higher peak intensity at 2.1 Å was obtained for nanosheets stored in NaAsc, suggesting a higher level of stability against oxidation.

(B and C) Final molecular configurations of $Ti_3C_2T_x$ nanosheet after 25-ps simulation of oxidation in water (B) and oxidation in the presence of NaAsc and water (C). L-Ascorbate group associates with the nanosheet (highlighted), restricting further reactions between the nanosheets and water molecules.

Molecular Simulations Show that Sodium L-Ascorbate Associates with Ti₃C₂T_x

ReaxFF molecular simulations were performed to elucidate the mechanism for NaAsc and ${\rm Ti_3C_2T_x}$ interactions. Two systems were examined: (1) a ${\rm Ti_3C_2T_x}$ nanosheet surrounded by water molecules, and (2) a ${\rm Ti_3C_2T_x}$ nanosheet with randomly placed NaAsc and water molecules. Both systems had a density of ~ 1 g/cm³. The starting nanosheet was populated with -OH terminal groups (Figure S7). The -F terminal groups were not considered for simulations because the current force field does not have well-defined Na-F interactions. ReaxFF simulations were carried out at 500°C with 0.25-fs time steps for 25 ps using large-scale atomic/molecular massively parallel simulation (LAMMPS)³¹ and the ReaxFF force field from Osti et al.³² It is computationally unfeasible to simulate the chemical kinetics of 21 days; therefore, the common method is to carry out the simulations at a higher temperature as compared with the experiments to accelerate the kinetics of the reaction.²⁴

To quantify the stability of the $Ti_3C_2T_x$ structures after oxidation, we carried out radial distribution function (rdf) calculations for the Ti-C atoms; these only consider the carbon atoms within the MXene structure. The radial distribution function, g(r), gives the probability of finding a particle at a distance r from another particle in 3D space. The rdf calculations were carried out for the last 10 ps of the simulations. Our results indicate substantially less oxidation when NaAsc is present in the system. The Ti-C rdf calculations show a peak at 2.1 Å (Figure 6A), which is characteristic for a crystalline $Ti_3C_2T_x$ structure. The Ti-C rdf peak intensity at 2.1 Å for the NaAsc system is higher than that of the water system, suggesting a more stable $Ti_3C_2T_x$ structure in the presence of NaAsc. The experimental XPS results also support this finding (Tables S2 and S3), as the atomic percentage of Ti-C is higher in $Ti_3C_2T_x$ stored in NaAsc as compared with $Ti_3C_2T_x$ stored in water.

The stability of the $Ti_3C_2T_x$ nanosheet (Figures 6B and 6C) can be attributed to the shielding of the $Ti_3C_2T_x$ structure by the ascorbate molecules that associate with the titanium atoms in the nanosheet. ³² The oxidized states of Ti (such as Ti^{3+} , Ti^{2+} , and TiO_2) are far less abundant in $Ti_3C_2T_x$ system simulated with NaAsc compared

Matter Cell^Press

with $Ti_3C_2T_x$ system simulated with water. During the simulation, the NaAsc loses the Na $^+$ cation, and the L-ascorbate anion associates with the nanosheet. The Ti-O bonding seen in the simulations primarily forms at the edges of the $Ti_3C_2T_x$ between the nanosheet and L-ascorbate. The L-ascorbate molecules associated with the nanosheet prevent nearby sites from interacting with water molecules, thereby locally shielding the nanosheet from oxidation. This is not true for the case of water oxidation, where water reacts with the nanosheet by breaking Ti-C bonds and forming Ti-O bonds in the process. The reaction between Ti and water subsequently creates more sites for oxidation, thereby reducing the size of the nanosheet. ReaxFF simulations also indicate preferred oxidation along the edges, in accordance with previous experimental observations. This can be attributed to the Ti atoms along the edges of nanosheet, which have significantly higher angle strain as compared with the Ti atoms in the basal plane. The final configurations of the simulation systems are presented in Figure S8.

Conclusion

This study demonstrates the relatively long-term stabilization of colloidal $Ti_3C_2T_x$ nanosheets in aqueous dispersion using NaAsc as the antioxidant. Without this antioxidant, the $Ti_3C_2T_x$ nanosheets rapidly degrade into TiO_2 , as shown by large-scale aggregation and a dramatic loss in conductivity of the $Ti_3C_2T_x$ film made from these samples. In contrast, the antioxidant enables $Ti_3C_2T_x$ nanosheets to retain their crystalline structure, morphology, colloidal stability, chemical composition, and electrical conductivity, even after 21 days in water. The origin of this stability against oxidation is attributed to the association of L-ascorbate anions to the edges of $Ti_3C_2T_x$ nanosheets, which prevent otherwise detrimental oxidation reactions. With these findings, shelf-stable MXenes become possible and engineering-grade MXenebased materials can become a practical reality.

EXPERIMENTAL PROCEDURES

Sample Preparation

Synthesis of Ti₃AlC₂ MAX Phase

Ti₃AlC₂ MAX phase was synthesized from Ti (with an average particle size of 44 μm and 99.5% purity), Al (with an average particle size of 44 μm and 99.5% purity), and TiC (with an average particle size of 2–3 μm and 99.5% purity) powders, which were weighed and mixed at the ratio of Ti/Al/C = 3.0:1.2:1.8. All chemicals were used as received from Alfa Aesar (MA, USA). To ensure the homogeneity of the blends, we mixed Ti, Al, and TiC powders in a laboratory ball mill filled with zirconia beads rotating at the speed of 300 rpm for 24 h. The bulk high-purity Ti₃AlC₂ samples were synthesized by sintering the powder mixture in a pressurized chamber of a pulsed electric current system at pressure of 50 MPa and temperature of 1,510°C for 15 min. After sintering, the bulk Ti₃AlC₂ samples were drill milled. The drill-milled MAX phase was sieved to obtain the powder with particle size less than 45 μm.

Synthesis of Ti₃C₂T_x MXene Clay

 ${\rm Ti_3C_2T_x}$ MXene clay was obtained by etching the Al layer from the MAX phase following a wet etching method described by Ghidiu et.al. First, 50 mL of 6 M hydrochloric acid (HCl) solution was prepared by diluting the concentrated HCl (37% [w/w], ACS reagent, Sigma-Aldrich) with deionized water. The 50 mL of 6 M HCL solution and 3.3 g of lithium fluoride (LiF) (with the purity of 98%+, Alfa Aesar) were mixed using a magnetic stir bar in a polytetrafluoroethylene (PTFE) bottle until all LiF was dissolved. The solution of HCl and LiF was heated to 40°C. Five grams of as-prepared MAX powder was slowly added into the solution over 15 min to prevent overheating (due to large exotherm of the etching reaction). The mixture was

Cell²ress

Matter

continuously agitated and reacted for 45 h. The suspension was then centrifuged and the supernatant (which contained the unreacted HF and water-soluble salt ions) was removed. Deionized water was used to wash the MXene clay in the sediments. The dispersion was then vigorously shaken and centrifuged to remove the water effluent. This step was repeated several times until the pH of the water effluent reached a minimum value of 6.

Synthesis of $Ti_3C_2T_x$ MXene Nanosheet Dispersion

As-prepared Ti₃C₂T_x MXene clay was intercalated with dimethyl sulfoxide (DMSO) (>99.5%, Sigma-Aldrich) and then bath sonicated to exfoliate into nanosheets.³³ One milliliter of DMSO was added to disperse every 60 mg of $Ti_3C_2T_x$ MXene clay. The MXene clay was intercalated at room temperature for 20 h with continuous magnetic stirring. After the intercalation, DMSO was removed by 3-4 cycles of solvent exchange with deionized water. The aqueous MXene clay dispersion was bath sonicated for 1 h to delaminate the multilayered MXene structures. The delaminated dispersion was centrifuged at 3,500 rpm for 1 h to crash out and separate the unexfoliated MXenes and other heavier components. The supernatant collected was the Ti₃C₂T_x nanosheet dispersion. The deionized water used in the steps described above had been purged with argon gas for at least 1 h to remove the dissolved oxygen to the maximum extent. A concentration of 6.06 mg/mL for the delaminated Ti₃C₂T_x nanosheet dispersion was determined by dividing the weight of freeze-dried nanosheets by the volume of MXene dispersion used for freeze dry. Thirty milliliters of the Ti₃C₂T_x nanosheet dispersion was frozen in liquid nitrogen and freeze-dried for at least 3 days to remove the moisture. The dried nanosheets were weighed by an electronic balance with an accuracy of 0.1 mg. The lateral size of the delaminated nanosheets is around 0.5-5 μm, verified by transmission electron microscopy.²²

Dilution of MXene Nanosheet Dispersion

For every 0.1 mL of as-prepared Ti₃C₂T_x nanosheet dispersion, premixed NaAsc stock solution was added to make a 100-mL dispersion with a NaAsc concentration of 1 mg/mL. Deionized water diluted nanosheet dispersions were prepared in the same way for reference purposes. The concentration of NaAsc in the diluted dispersion was maintained at 1 mg/mL for maintaining the MXene colloidal stability.

Vacuum Filtration

The macroassemblies of layered Ti₃C₂T_x nanosheets were made by vacuum filtration of MXene dispersion using Supor Polyethersulfone Membrane (Pall Laboratory). The MXene nanosheets were pretreated by antioxidants such as sodium L-ascorbate, tannic acid, and ascorbic acid at desired concentrations. The filtered films were then vacuum dried after filtration at 40°C for 12 h.

X-Ray Diffraction

XRD patterns of dried Ti₃C₂T_x were obtained using Bruker D8 powder X-ray diffractometer fitted with LynxEye detector, in a Bragg Brentano geometry with CuKa $(\lambda = 1.5418 \text{ Å})$ radiation source. The X-ray scan was performed with a step size of 0.02° and a scan rate of 1.5 s per step. The $\text{Ti}_3\text{C}_2\text{T}_x$ samples were freeze-dried before the XRD measurements. A zero-background sample holder was used in all the tests.

Dynamic Light Scattering

The average hydrodynamic diameters of aqueous ${\rm Ti_3C_2T_x}$ nanosheets were determined at ambient temperature by DLS at a scattering angle of 90° using a Zetasizer Nano ZS90 from Malvern Instruments (UK). The colloidal aqueous dispersion of Ti₃C₂T_x nanosheets was diluted to a concentration of around 0.006 mg/mL before



measurements to ensure consistency. Each test was repeated at least six times, and an average value was derived to ensure accuracy.

C-Potential Measurement

 ζ -Potential changes of Ti₃C₂T_x nanosheets in water and NaAsc solution were probed at ambient temperature using the Zetasizer Nano ZS90 from Malvern Instruments and the appropriate capillary cell, DTS 1070, from Malvern Instruments. The colloid of Ti₃C₂T_x nanosheets was diluted to a concentration around 0.006 mg/mL before measurements to ensure consistency. Each test was repeated at least six times and an averaged value was derived to ensure accuracy.

X-Ray Photoelectron Spectroscopy

The surface chemistry of as-prepared and stored $Ti_3C_2T_x$ nanosheets was probed using an Omicron X-ray photoelectron spectrometer employing a Mg-sourced X-ray beam to irradiate the sample surface. The emitted photoelectrons from the sample surface were collected by a 180° hemispherical electron energy analyzer. A takeoff angle of 40° between sample surface and the path to the photoelectron collector was used in all measurements. During all scanning, charge neutralization by a dual-beam charge neutralizer was performed to irradiate the low-energy electrons to eliminate the binding energy (BE) shifts in the recorded spectra. Samples for XPS measurements were prepared by repeatedly drop-casting the $Ti_3C_2T_x$ dispersion onto hydrophilic silicon wafer, which was pretreated in an oxygen plasma cleaner. The samples were then dried under vacuum at 40° C for 12 h to prevent any outgassing. High-resolution spectra of Ti 2p, C 1s, O 1s, and F 1s were recorded at a pass energy (constant analyzer energy) of 30.0 eV with a step size of 0.05 eV.

Component peak fitting and quantification of the spectra were carried out using CasaXPS curve fitting software (version 2.3.16). Prior to peak fitting, a region was created for each entry. The background contributions were subtracted by applying a Shirley type background function. All spectra were charge calibrated based on the adventitious C 1s component (C-C) with a BE of 284.8 eV. Peak fitting was performed using symmetric Gaussian-Lorentzian curves (GL30). A few rigid constraints were imposed during peaking fitting to ensure reasonable and consistent results with the literature. First, for all $2p_{3/2}$ and $2p_{1/2}$ components in the titanium spectra, the peak area ratios were constrained to be fixed exactly at 2:1 (2p_{3/2}:2p_{1/2}) as given by quantum mechanics selection rules. In addition, the full width at half maximum (FWHM) of each component was restricted. The same component present in each sample was expected to exhibit only small variations in the FWHM. The BE and delta values for 2p_{3/2}-2p_{1/2} splitting for each component were constrained according to a series of literature and NIST XPS database reported values. 11,34-36 The standard deviations for the fitted components were computed using the Monte Carlo error analysis built into the CasaXPS software. The standard deviations of the fittings were found to range between 0.1% and 5.0% for all stated components.

The Ti 2p region was deconvoluted into five pairs of the $2p_{3/2}$ and $2p_{1/2}$ spin-orbit split components, which were assigned to Ti-C, Ti(II), Ti(III), Ti(IV), and Ti-F, respectively. Note that for the MXene sample stored in water, since the atomic percentage of fluorine became very low, the Ti-F curves were neglected in the fitting. The C 1s spectrum was deconvoluted into six components, namely C-C, C-Ti-T_{x1}, C-Ti-T_{x2}, CH_x/CO, C-OH, and COO, respectively. The O 1s spectrum was deconvoluted into five components, namely TiO₂, C-Ti-O_x, C-Ti-(OH)_x, Al₂O₃, and H₂O. The F 1s spectrum was deconvoluted into two components: AlF_x and C-Ti-F_x.

Scanning Electron Microscopy

The morphologies of Ti₃C₂T_x nanosheets after storage were observed with an FEI Quanta 600 field-emission scanning electron microscope. For imaging, the vigorously mixed dispersions of stored Ti₃C₂T_x nanosheets were drop-casted on hydrophilic silicon wafers pretreated with oxygen plasma and then vacuum dried. The acceleration voltage used in the imaging was 2 kV.

Conductivity Measurement

The electrical conductivity was measured using four-point resistivity probe powered by Keithley Instruments models, one 2000, one 6221, and two 6514. MXene films used for the conductivity measurements were prepared by vacuum filtering the $Ti_3C_2T_x$ nanosheet dispersions as described above.

Simulation Setup

ReaxFF is a reactive force-field molecular dynamics simulation technique that uses the bond-order concept to compute the interaction between atoms at each time step.³⁷ Compared with other non-reactive atomistic simulation techniques, ReaxFF provides a smooth transition between the non-bonded states and the bonded states. In general, the total energy of the system in ReaxFF is described by several contributions and can be summed up as follows:

$$E_{system} = E_{bond} + E_{over} + E_{under} + E_{val} + E_{tors} + E_{vdw} + E_{Coulomb} + E_{lp} + E_{H-bond}$$
. (Equation 1)

The total energy of the system (E_{system}) consists of bond-order-dependent or covalent interactions and non-bonded interactions. Bond-order-dependent terms include the bond energy ($E_{\rm bond}$), overcoordination ($E_{\rm over}$), undercoordination (E_{under}), and hydrogen bond (E_{H-bond}) interactions. Energy penalty terms include torsion angle energy (E_{tor}), valence angle energy (E_{val}), and lone pair energy (E_{lp}) , whereas the non-bonded interactions are van der Waals energy (E_{vdw}) and Coulomb energy (E_{Coulomb}). At every time step, bond order between all pairs of atoms is calculated from their interatomic distances and updated. Also, nonbonded interactions such as van der Waals and Coulomb terms are considered for all atom pairs. Force-field parameters describing energy terms are typically optimized by quantum mechanics calculations. The force field used in the current investigation has been fitted for Ti- and C-based MXene structure and has shown good correlation with experiments.32

Two systems were generated, the first with 200 water molecules and a single $Ti_3C_2(OH)$ structure, and the second system had 50 NaAsc molecules added to it. The water and the NaAsc molecules were randomly distributed around the MXene structure. The molecular structure of Ti₃C₂(OH) and NaAsc are provided in Figure S7. The density of both the systems was kept at ~1 g/mL. NVT simulations were carried out 500°C (773 K) with 0.25-fs time steps for a total time of 25 ps using LAMMPS.³¹ Simulations were carried at elevated temperatures as compared with the experiments to accelerate the kinetics of the reactions. Although parameters for Ti-F are defined in the current force field,³² the F group was neglected as Na-F force-field parameters were not well defined. rdf calculations were carried out using VMD (Visual Molecular Dynamics)³⁸ for the last 10 ps of the oxidation simulations.

SUPPLEMENTAL INFORMATION

Supplemental Information can be found online at https://doi.org/10.1016/j.matt. 2019.05.020.



ACKNOWLEDGMENTS

Funding supporting this work was provided by the US National Science Foundation (grant CMMI-1760859). We would like to acknowledge Dr. Mustafa Akbulut's group and graduate student Shuhao Liu at Texas A&M University for assistance in the use of their Zetasizer instrument. We acknowledge the TAMU Materials Characterization Facility for use of XPS and scanning electron microscopy, and TAMU Department of Chemistry for use of XRD. The assistance from Dr. Jing Wu in the Materials Characterization Facility at Texas A&M University for XPS measurement is acknowledged. Portions of this research were conducted with the advanced computing resources provided by High Performance Research Computing at Texas A&M University.

AUTHOR CONTRIBUTIONS

Conceptualization: M.J.G., J.L.L., M.R., X.Z., S.A.S., and W.S.; Methodology, M.J.G., X.Z., A.V., S.A.S., and T.H.; Investigation, X.Z., E.P., Y.C., and Z.T.; Formal Analysis, A.V.; Writing - Original Draft, X.Z., A.V., and M.J.G.; Writing - Review & Editing, M.J.G., J.L.L., M.R., X.Z., and A.V.; Supervision, M.J.G., J.L.L., and M.R.

DECLARATION OF INTERESTS

The authors declare no competing financial interests.

Received: January 17, 2019 Revised: April 10, 2019 Accepted: May 16, 2019 Published: June 26, 2019

REFERENCES

- 1. Naguib, M., Mashtalir, O., Carle, J., Presser, V., Lu, J., Hultman, L., Gogotsi, Y., and Barsoum, M.W. (2012). Two-dimensional transition metal carbides. ACS Nano 6, 1322-1331.
- 2. Naguib, M., Mochalin, V.N., Barsoum, M.W., and Gogotsi, Y. (2014). 25th anniversary article: MXenes: a new family of two-dimensional materials. Adv. Mater. 26, 992-1005.
- 3. Dillon, A.D., Ghidiu, M.J., Krick, A.L., Griggs, J., May, S.J., Gogotsi, Y., Barsoum, M.W., and Fafarman, A.T. (2016). Highly conductive optical quality solution-processed films of 2D titanium carbide. Adv. Funct. Mater. 26, 4162-4168.
- 4. Peng, X., Peng, L., Wu, C., and Xie, Y. (2014). Two dimensional nanomaterials for flexible supercapacitors. Chem. Soc. Rev. 43, 3303-
- 5. An, H., Habib, T., Shah, S., Gao, H., Radovic, M., Green, M.J., and Lutkenhaus, J.L. (2018). Surface-agnostic highly stretchable and bendable conductive MXene multilayers. Sci. Adv. 4, eaaq0118.
- 6. Shahzad, F., Alhabeb, M., Hatter, C.B., Anasori, B., Man Hong, S., Koo, C.M., and Gogotsi, Y. (2016). Electromagnetic interference shielding with 2D transition metal carbides (MXenes). Science 353, 1137-1140.
- 7. Han, M., Yin, X., Wu, H., Hou, Z., Song, C., Li, X., Zhang, L., and Cheng, L. (2016). Ti₃C₂ MXenes with modified surface for high-performance electromagnetic absorption and shielding in

- the X-band. ACS Appl. Mater. Interfaces 8, 21011-21019.
- 8. Er, D., Li, J., Naguib, M., Gogotsi, Y., and Shenoy, V.B. (2014). Ti₃C₂ MXene as a high capacity electrode material for metal (Li, Na, K, Ca) ion batteries. ACS Appl. Mater. Interfaces 6, 11173-11179.
- 9. Yuan, W., Cheng, L., An, Y., Wu, H., Yao, N., Fan, X., and Guo, X. (2018). MXene nanofibers as highly active catalysts for hydrogen evolution reaction. ACS Sustain. Chem. Eng. 6, 8976-8982.
- 10. Seh, Z.W., Fredrickson, K.D., Anasori, B., Kibsgaard, J., Strickler, A.L., Lukatskaya, M.R., Gogotsi, Y., Jaramillo, T.F., and Vojvodic, A (2016). Two-dimensional molybdenum carbide (MXene) as an efficient electrocatalyst for hydrogen evolution. ACS Energy Lett. 1,
- 11. Shah, S.A., Habib, T., Gao, H., Gao, P., Sun, W., Green, M.J., and Radovic, M. (2017). Templatefree 3D titanium carbide (Ti₃C₂T_x) MXene particles crumpled by capillary forces. Chem. Commun. (Camb.) 53, 400-403.
- 12. Naguib, M., Kurtoglu, M., Presser, V., Lu, J., Niu, J., Heon, M., Hultman, L., Gogotsi, Y., and Barsoum, M.W. (2011). Two-dimensional nanocrystals produced by exfoliation of Ti₃AlC₂. Adv. Mater. 23, 4248–4253.
- 13. Eklund, P., Rosen, J., and Persson, P.O.Å. (2017). Layered ternary Mn+1AXn phases and their 2D derivative MXene: an overview from a

- thin-film perspective. J. Phys. D Appl. Phys. 50, 113001.
- 14. Ghidiu, M., Lukatskaya, M.R., Zhao, M.-Q., Gogotsi, Y., and Barsoum, M.W. (2014). Conductive two-dimensional titanium carbide 'clay' with high volumetric capacitance. Nature 516, 78-81.
- 15. Sun, W., Shah, S.A., Chen, Y., Tan, Z., Gao, H., Habib, T., Radovic, M., and Green, M.J. (2017). Electrochemical etching of Ti₂AIC to Ti₂CT_x (MXene) in low-concentration hydrochloric acid solution. J. Mater. Chem. A 5, 21663-21668.
- 16. Alhabeb, M., Maleski, K., Anasori, B., Lelyukh, P., Clark, L., Sin, S., and Gogotsi, Y. (2017) Guidelines for synthesis and processing of twodimensional titanium carbide (Ti₃C2T_x MXene). Chem. Mater. 29, 7633-7644.
- 17. Hong Ng, V.M., Huang, H., Zhou, K., Lee, P.S., Que, W., Xu, J.Z., and Kong, L.B. (2017). Recent progress in layered transition metal carbides and/or nitrides (MXenes) and their composites: synthesis and applications. J. Mater. Chem. A. 5, 3039-3068.
- 18. Lipatov, A., Alhabeb, M., Lukatskaya, M.R., Boson, A., Gogotsi, Y., and Sinitskii, A. (2016). Effect of synthesis on quality, electronic properties and environmental stability of individual monolayer Ti₃C₂ MXene flakes. Adv. Electron. Mater. *2*, 1600255.
- 19. Mashtalir, O., Cook, K.M., Mochalin, V.N., Crowe, M., Barsoum, M.W., and Gogotsi, Y (2014). Dye adsorption and decomposition on



- two-dimensional titanium carbide in aqueous media. J. Mater. Chem. A 2, 14334-14338.
- Zhang, C.J., Pinilla, S., McEvoy, N., Cullen, C.P., Anasori, B., Long, E., Park, S.H., Seral-Ascaso, A., Shmeliov, A., Krishnan, D., et al. (2017). Oxidation stability of colloidal twodimensional titanium carbides (MXenes). Chem. Mater. 29, 4848-4856.
- 21. Ghassemi, H., Harlow, W., Mashtalir, O., Beidaghi, M., Lukatskaya, M.R., Gogotsi, Y., and Taheri, M.L. (2014). In situ environmental transmission electron microscopy study of oxidation of two-dimensional Ti₃C₂ and formation of carbon-supported TiO_2 . J. Mater. Chem. A 2, 14339-14343.
- 22. Habib, T., Zhao, X., Shah, S.A., Chen, Y., Sun, W., An, H., Lutkenhaus, J.L., Radovic, M., and Green, M.J. (2019). Oxidation stability of Ti₃C₂T_x MXene nanosheets in solvents and composite films. NPJ 2D Mater. Appl. 3, 8.
- 23. Maleski, K., Mochalin, V.N., and Gogotsi, Y. (2017). Dispersions of two-dimensional titanium carbide MXene in organic solvents. Chem. Mater. 29, 1632-1640.
- 24. Lotfi, R., Naguib, M., Yilmaz, D.E., Nanda, J., and van Duin, A.C.T. (2018). A comparative study on the oxidation of two-dimensional Ti₃C₂ MXene structures in different environments. J. Mater. Chem. A 6, 12733-
- 25. Anasori, B., Lukatskaya, M.R., and Gogotsi, Y. (2017). 2D metal carbides and nitrides

- (MXenes) for energy storage. Nat. Rev. Mater. 2. 16098
- 26. Liang, X., Rangom, Y., Kwok, C.Y., Pang, Q., and Nazar, L.F. (2017). Interwoven MXene nanosheet/carbon-nanotube composites as Li-S cathode hosts. Adv. Mater. 29, 1603040.
- 27. Huang, S., and Mochalin, V.N. (2019). Hydrolysis of 2D transition-metal carbides (MXenes) in colloidal solutions. Inorg. Chem. 58, 1958–1966.
- 28. Wu, X., Wang, Z., Yu, M., Xiu, L., and Qiu, J. (2017). Stabilizing the MXenes by carbon nanoplating for developing hierarchical nanohybrids with efficient lithium storage and hydrogen evolution capability. Adv. Mater. 29, 1607017.
- 29. Li, Z., Wang, L., Sun, D., Zhang, Y., Liu, B., Hu, Q., and Zhou, A. (2015). Synthesis and thermal stability of two-dimensional carbide MXene Ti₃C₂. Mater. Sci. Eng. C 191, 33–40.
- 30. Liu, R., and Li, W. (2018). High-thermal-stability and high-thermal-conductivity $Ti_3C_2T_x$ MXene/ Poly(vinyl alcohol) (PVA) composites. ACS Omega 3, 2609-2617.
- 31. Plimpton, S. (1995). Fast parallel algorithms for short-range molecular-dynamics. J. Comput. Phys. 117, 1-19.
- 32. Osti, N.C., Naguib, M., Ostadhossein, A., Xie, Y., Kent, P.R.C., Dyatkin, B., Rother, G., Heller, W.T., van Duin, A.C., Gogotsi, Y., et al. (2016). Effect of metal ion intercalation on the

- structure of MXene and water dynamics on its internal surfaces. Acs Appl. Mater. Interfaces 8, 8859-8863.
- 33. Mashtalir, O., Naguib, M., Mochalin, V.N., Dall'Agnese, Y., Heon, M., Barsoum, M.W., and Gogotsi, Y. (2013). Intercalation and delamination of layered carbides and carbonitrides. Nat. Commun. 4, 1716.
- 34. Halim, J., Cook, K.M., Naguib, M., Eklund, P., Gogotsi, Y., Rosen, J., and Barsoum, M.W. (2016). X-ray photoelectron spectroscopy of select multi-layered transition metal carbides (MXenes). Appl. Surf. Sci. 362, 406-417.
- 35. Halim, J., Lukatskaya, M.R., Cook, K.M., Lu, J., Smith, C.R., Näslund, L.-A., May, S.J., Hultman, L., Gogotsi, Y., Eklund, P., et al. (2014). Transparent conductive two-dimensional titanium carbide epitaxial thin films. Chem. Mater. 26, 2374-2381.
- 36. Biesinger, M.C., Lau, L.W.M., Gerson, A.R., and Smart, R.S.C. (2010). Resolving surface chemical states in XPS analysis of first row transition metals, oxides and hydroxides: Sc, Ti, V, Cu and Zn. Appl. Surf. Sci. 257, 887-898.
- 37. van Duin, A.C.T., Dasgupta, S., Lorant, F., and Goddard, W.A. (2001). ReaxFF: a reactive force field for hydrocarbons. J. Phys. Chem. A 105, 9396-9409.
- 38. Humphrey, W., Dalke, A., and Schulten, K. (1996). VMD: Visual Molecular Dynamics. J. Mol. Graph. 14, 33-38.

Supplemental Information

Antioxidants Unlock Shelf-Stable

Ti₃C₂T_x (MXene) Nanosheet Dispersions

Xiaofei Zhao, Aniruddh Vashisth, Evan Prehn, Wanmei Sun, Smit A. Shah, Touseef Habib, Yexiao Chen, Zeyi Tan, Jodie L. Lutkenhaus, Miladin Radovic, and Micah J. Green

Supplemental Information

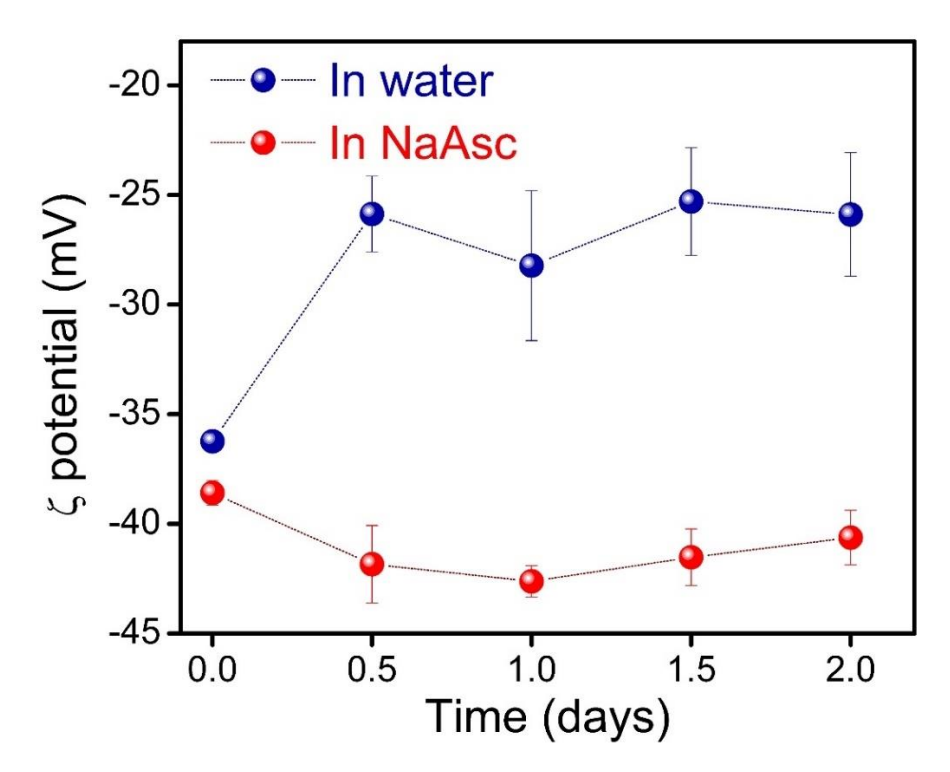


Figure S1 Zeta (ζ) potential changes of $Ti_3C_2T_x$ nanosheets dispersed in deionized water and 1 mg/mL sodium L-ascorbate solution (NaAsc) in the first 2 days of storage. A dramatic increase of ζ potential of $Ti_3C_2T_x$ MXene nanosheets/water dispersion is observed in the first 12 hours; in contrast, NaAsc stabilizes the colloidal dispersion and shows a relatively stable ζ potential.

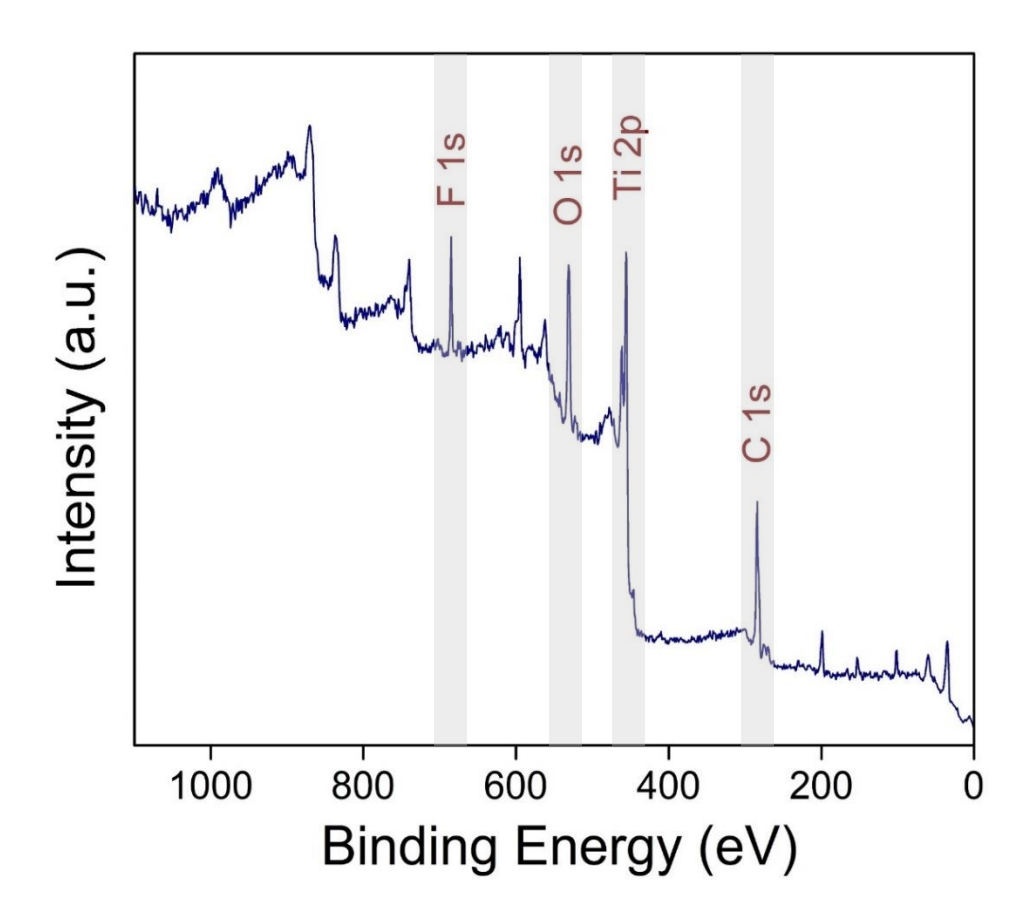


Figure S2 XPS survey spectrum of as-prepared $Ti_3C_2T_x$ nanosheets dried after delamination labelled with characteristic peaks of Ti 2p, C 1s, O 1s, and F 1s.

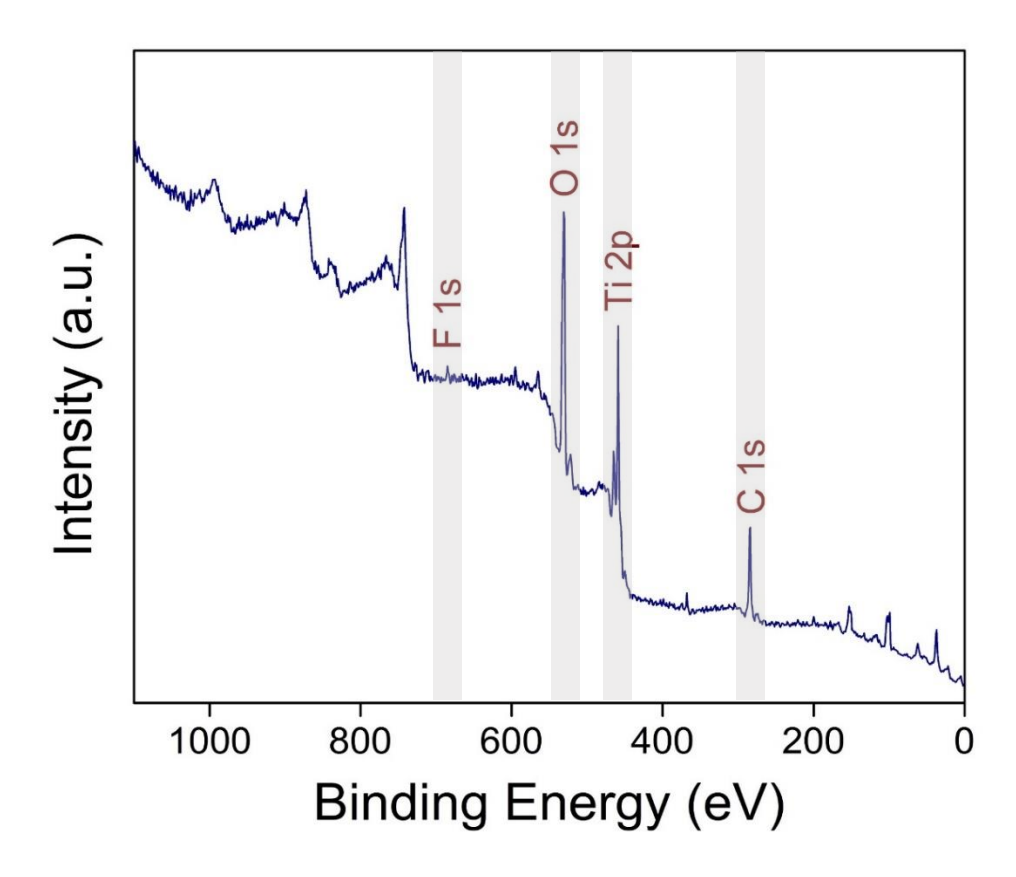


Figure S3 XPS survey spectrum of the $Ti_3C_2T_x$ MXene nanosheets drop-cast and dried after being stored in deionized water for 21 days, labelled with characteristic peaks of Ti 2p, C 1s, O 1s, and F 1s. The F 1s peak is no longer prominent in this survey spectrum due to oxidation and degradation of the MXene structure.

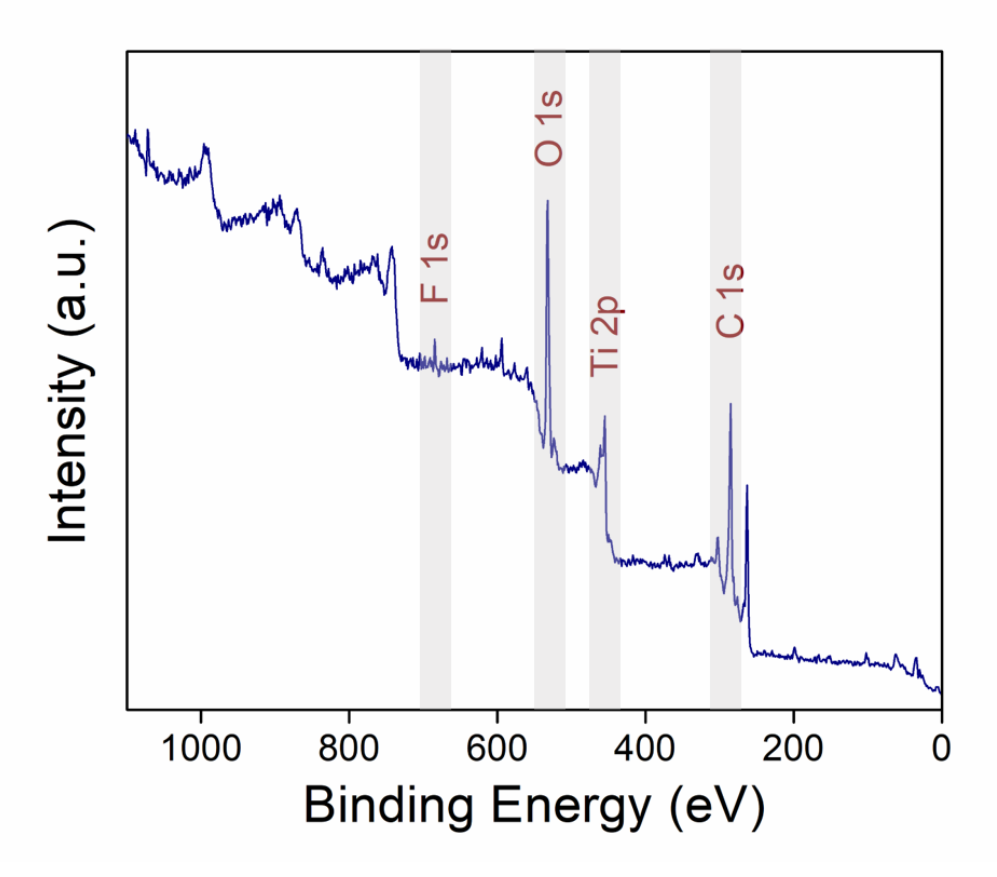


Figure S4 XPS survey spectrum of the $Ti_3C_2T_x$ nanosheets dried after being stored in sodium L-ascorbate solution (1 mg/mL) for 21 days, labelled with characteristic peaks of Ti 2p, C 1s, O 1s, F 1s and Na 1s (from sodium L-ascorbate).

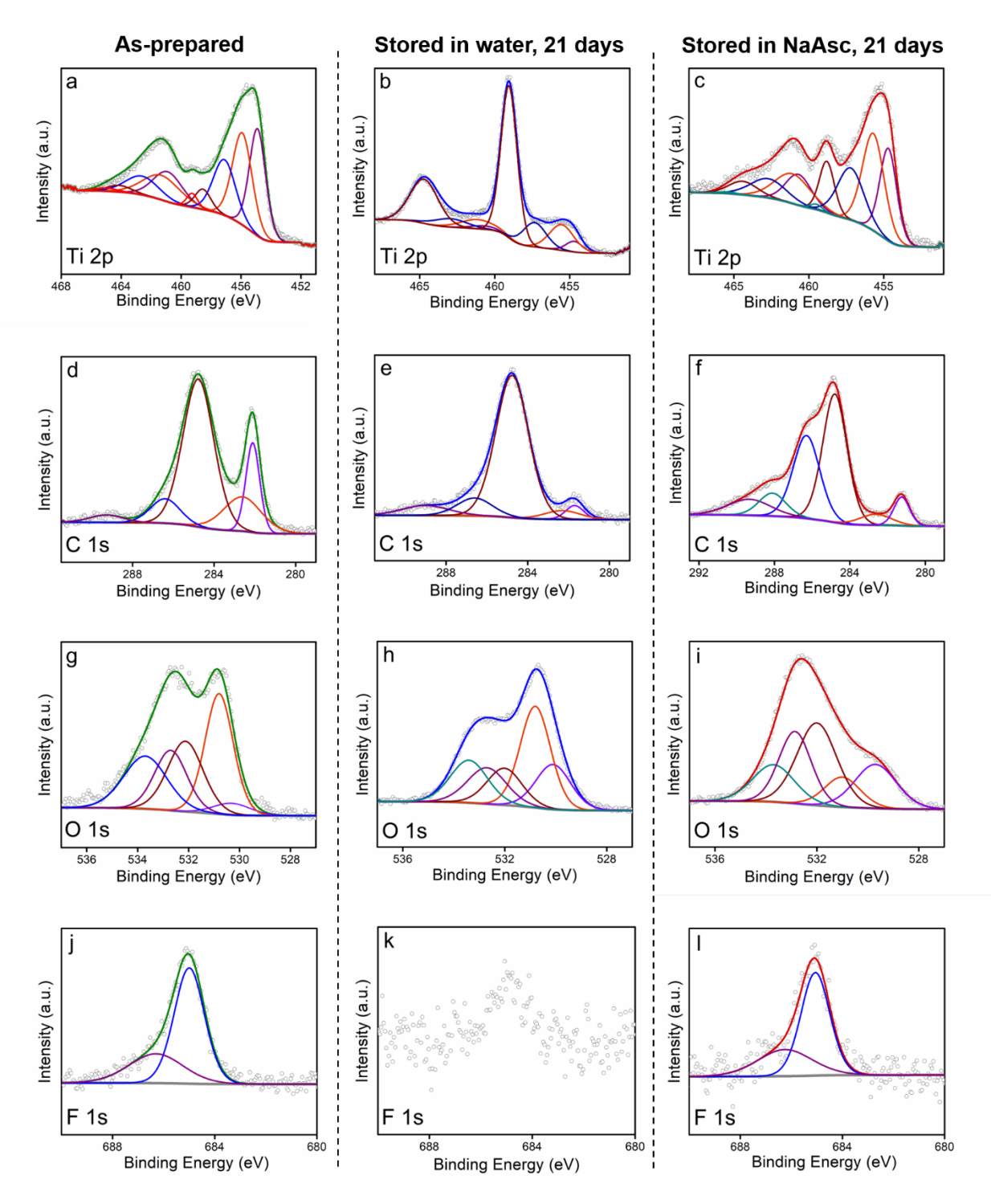


Figure S5 Component peak fittings of XPS spectra for as-prepared $Ti_3C_2T_x$ nanosheets and nanosheets after being stored in deionized water and sodium L-ascorbate solution (1 mg/mL) for 21 days.

Table S1 XPS peak fitting results for as-prepared Ti₃C₂T_x MXenes.

Element	Element atomic%	Binding energy (BE) (eV) Component name Component atomic%		-	FWHM
Ti 2p _{3/2} (2p _{1/2})	18.5	454.9 (460.9)	Ti-C	33.2	1.3 (2.3)
		455.9 (461.4)	Ti ²⁺	34.4	1.5 (2.9)
		457.1 (462.6)	Ti ³⁺	23.5	1.7 (2.6)
		458.5 (464.1)	TiO ₂	6.1	1.2 (1.9)
		459.3 (465.1)	Ti-F _x	2.9	0.9 (1.9)
	52.3	282.1	C-Ti-T _x ^a	15.3	0.8
		282.6	C-Ti-T _x ^a	16.1	2.2
C 1s		284.8	C-C	56.6	1.8
		286.4	CH _x /CO	8.9	1.7
		289.3	COO	3.1	1.9
O 1s	22.4	530.3	TiO ₂	4.1	1.7
		530.8	C-Ti-O _x	32.1	1.3
		532.1	C-Ti-(OH) _x	23.7	1.6
		532.7	Al ₂ O ₃	18.5	1.5
		533.7	H ₂ O ^b	21.6	2.0
F 1s	6.8	685.0	C-Ti-F _x	68.9	1.4
		686.3	AlF _x	31.1	2.5

 $^{^{}a}$ T_{x} represents the terminal groups grafted on the $Ti_{3}C_{2}T_{x}$ MXene nanosheets. The peak corresponding to this bond is asymmetric, so it is represented by two symmetric peaks.

^b Water molecules associated with terminal group -OH.

 $\textbf{Table S2} \ \text{XPS peak fitting results for } Ti_3C_2T_x \ \text{MXene nanosheets after being stored in deionized }$ water.

Element	Element atomic%	Binding energy (BE) (eV)	Component name	Component atomic%	FWHM
	14.0	454.7 (460.7)	Ti-C	4.6	1.3 (2.0)
Ti 2p _{3/2}		455.5 (461.1)	Ti ²⁺	16.2	1.9 (2.6)
$(2p_{1/2})$		457.3 (462.9)	Ti ³⁺	14.6	1.8 (2.6)
		459.0 (464.7)	TiO ₂	64.6	1.3 (2.2)
		281.7	C-Ti-T _x ^a	4.0	1.0
	40.0	282.3	C-Ti-T _x ^a	5.0	2.1
C 1s		284.8	C-C	73.8	1.9
		286.6	CH _x /CO	9.9	2.0
		289.0	COO	7.3	2.7
O 1s	45.8	530.1	TiO ₂	17.2	1.6
		530.8	C-Ti-O _x	34.4	1.5
		532.0	C-Ti-(OH) _x	14.6	1.8
		532.7	Al ₂ O ₃	16.1	1.8
		533.4	H ₂ O ^b	17.7	1.8
F 1s	0.2	N/A	N/A	N/A	N/A

 $^{^{}a}$ T_x represents the terminal groups grafted on the Ti₃C₂T_x MXene nanosheets. The peak corresponding to this bond is asymmetric, so it is represented by two symmetric peaks. b Water molecules associated with terminal group -OH.

Table S3 XPS peak fitting results for $Ti_3C_2T_x$ MXene nanosheets after being stored in sodium L-ascorbate solution (1 mg/mL).

Element	Element atomic%	Binding energy (BE) (eV) Component name Component atomic%		FWHM	
Ti 2p _{3/2} (2p _{1/2})	6.9	454.7 (460.7)	Ti-C	26.8	1.3 (2.0)
		455.7 (461.1)	Ti ²⁺	36.0	1.7 (2.8)
		457.2 (462.7)	Ti ³⁺	23.2	1.9 (2.8)
		458.8 (464.4)	TiO ₂	13.1	1.2 (2.2)
		459.5 (465.5)	Ti-F _x	1.0	0.9 (1.5)
	63.6	281.2	C-Ti-T _x ^a	6.0	1.0
		282.6	C-Ti-T _x ^a	4.7	2.0
C 1s		284.8	C-C	42.1	1.5
CIS		286.3	CH _x /CO	29.6	1.6
		288.1	C-OH ^b	8.3	1.7
		289.3	COO	9.3	2.6
O 1s	28.1	529.7	TiO ₂	18.2	1.9
		531.0	C-Ti-O _x	10.7	1.7
		532.0	C-Ti-(OH) _x	32.5	1.8
		532.9	Al ₂ O ₃	23.1	1.5
		533.7	H ₂ O ^c	15.5	1.9
F 1s	1.5	685.1	C-Ti-F _x	67.4	1.3
		686.3	AlF _x	32.6	2.5

^a T_x represents the terminal groups grafted on the Ti₃C₂T_x MXene nanosheets. The peak corresponding to this bond is asymmetric, so it is represented by two symmetric peaks. ^b NaAsc associated with MXene nanosheets. ^c Water molecules associated with terminal group -OH.

 $\begin{tabular}{ll} \textbf{Table S4} Electrical conductivities of buckypapers made from as-prepared MXenes and stored \\ Ti_3C_2T_x MXenes in deionized water and 1 mg/mL sodium L-ascorbate solution. \\ \end{tabular}$

No. of days	In deionized water (S/m)	In 1 mg/mL NaAsc (S/m)
0	$3.2 \pm 0.3 \times 10^5$	$2.2 \pm 0.2 \times 10^5$
21	<10 ⁻⁶	$5.7 \pm 0.5 \times 10^4$

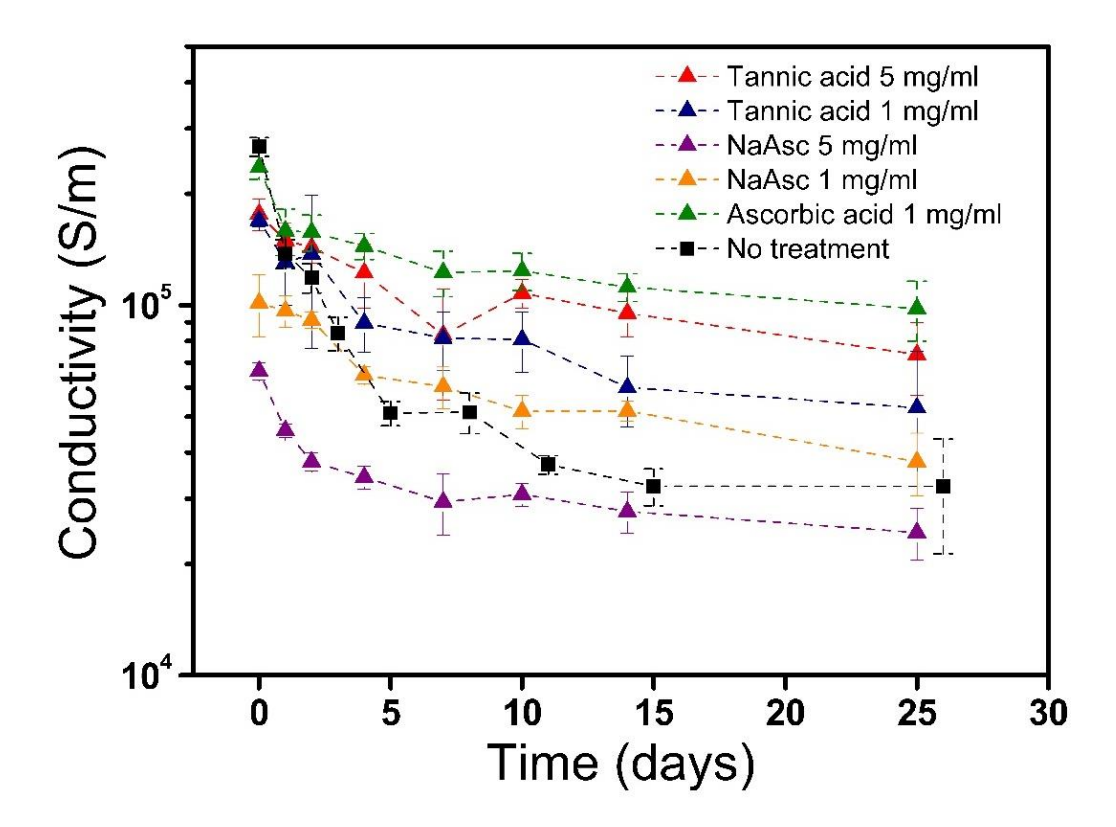


Figure S6 Conductivity changes were measured for dried films made from $Ti_3C_2T_x$ nanosheets pretreated by various antioxidants. The decreasing rates of the electrical conductivity for buckypapers made from pretreated nanosheets are much lower than the sample made from pristine nanosheets. The differences among the initial conductivities were possibly caused by the effects of slight antioxidant attachments and antioxidant adsorption due to the electronegativity of $Ti_3C_2T_x$ nanosheets.

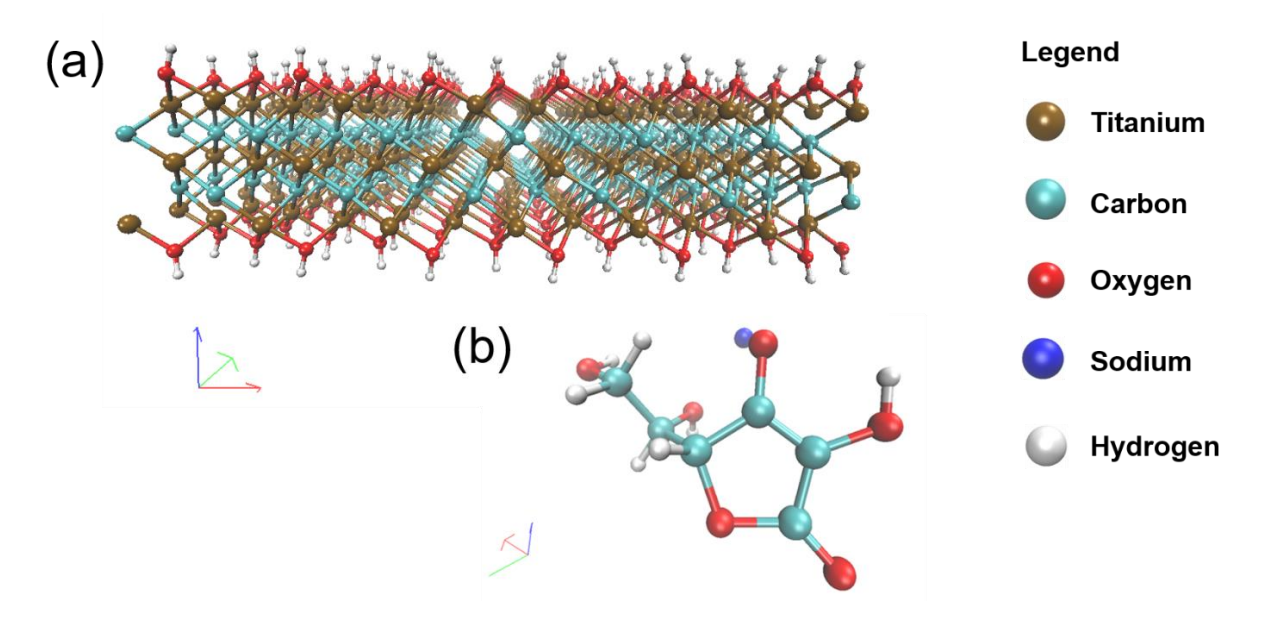


Figure S7 Molecular structure of (a) Ti₃C₂(OH) MXene nanosheet and (b) Sodium L-ascorbate (C₆H₇O₆Na) molecule, used for reactive molecular dynamic simulations.

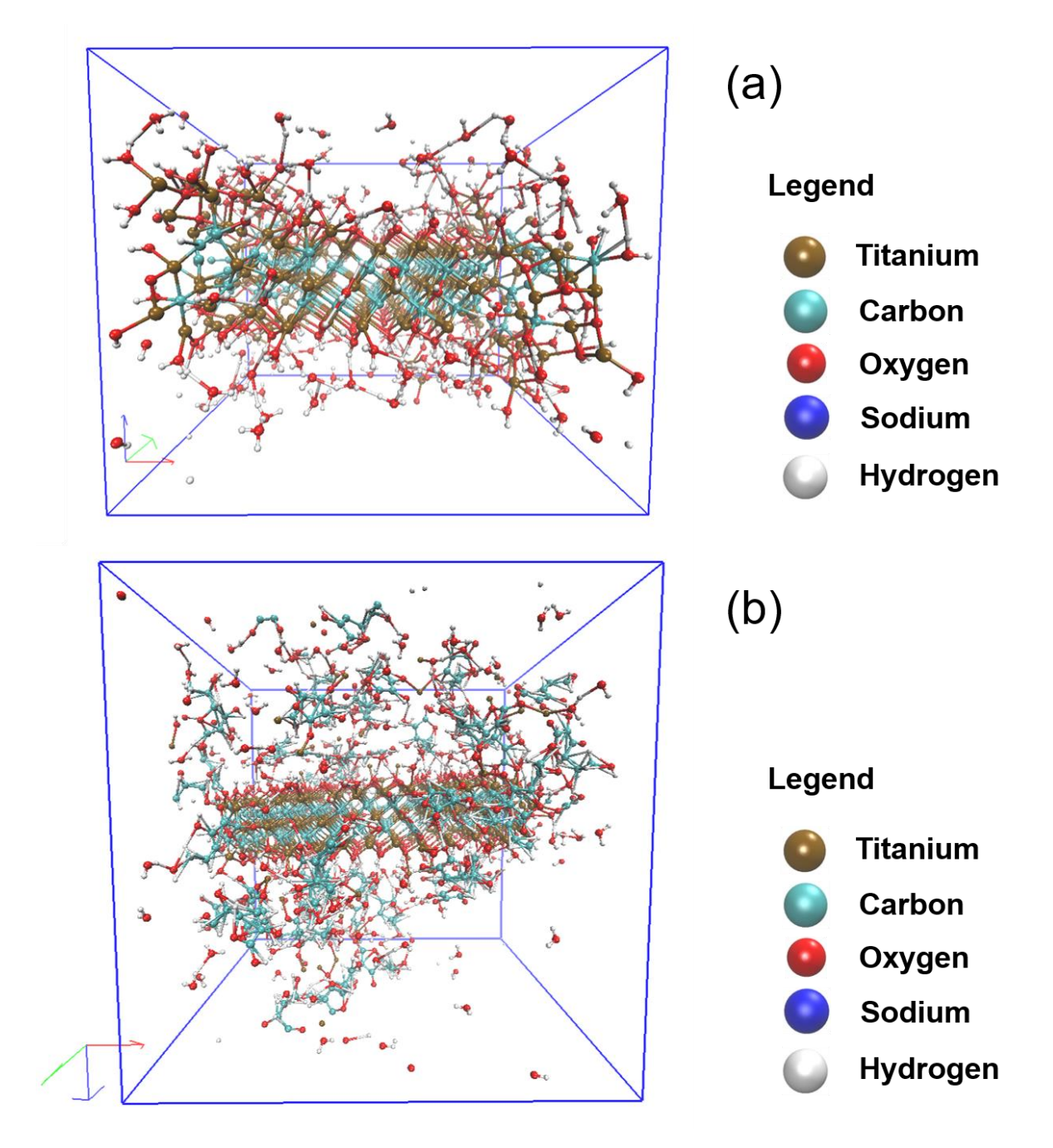


Figure S8 Final molecular configuration of molecules after 25 ps of molecular dynamic simulation of systems with (a) $Ti_3C_2T_x$ MXene nanosheet and water, and (b) $Ti_3C_2T_x$ MXene nanosheet, water and NaAsc. The solid line represents the box dimensions for the reaction.

Note: The mechanism of NaAsc minimizing $Ti_3C_2T_x$ oxidation is significantly different from the metal ion intercalation for better stability of $Ti_3C_2T_x$ as suggested by Osti *et al.* [1]. The metal

 (K^+) intercalation method found that water in between the individual MXene layers becomes much less mobile due to the presence of K^+ ions, thereby increasing the stability of the composite 2D material against the changes in the environmental conditions.

Simulation of nanosheet-cation interactions

We carried out molecular dynamics simulations to address the interactions of both sodium cations and the dissociated ascorbate group with the nanosheets. The simulations probe a 25 ps timeframe with MXene, NaAsc, and water; the frames from the first and last 0.75 ps of the 25 ps of simulations were used for rdf calculations. While carrying out rdf calculations for Na-O, only the oxygen atoms (O) on the basal plane of nanosheet were considered for the calculations. The oxygen atoms in water and ascorbate molecules were not considered for rdf calculations. Figure S9 shows that the initial 0.75 ps of the simulations do not exhibit a peak at 2 Å (bond length of Na-O bond), suggesting no association between Na⁺ and O at the beginning of the simulation. A weak peak is seen at the end of the 0.75 ps of the simulation at 2 Å, suggesting minor quantities of association between Na⁺ and O. To quantify this association, we calculated the number integral $(\int_0^r \rho g(r) r^2 dr)$ for all Na-O atomic pairs (where ρ is density, g(r) is rdf and r is inter-atomic distance). This number integral of g(r) for Na-O is the number of Na cations found within radius r of an O atom, which can also be described as a coordination number for selected bond types. Figure S10 shows int [g(r)] for Na-O atom pair, the inset shows the magnified values between 1.5 -3 Å. From these int [g(r)] calculations we observe a very small change in coordination number at ~2 Å, suggesting a very limited degree of Na-O association. It should also be noted that the simulations considered only -OH functionality in MXene (due to limitations of force field parameters), whereas the experiments suggest that other functionalities are also present in the basal

plane. Therefore, in experiments, we should potentially observe much smaller Na-O interactions. The simulation results indicate that the majority of Na is free-moving in the water at a low concentration of sodium L-ascorbate during the MXene storage, only the ascorbate groups interact with MXenes.

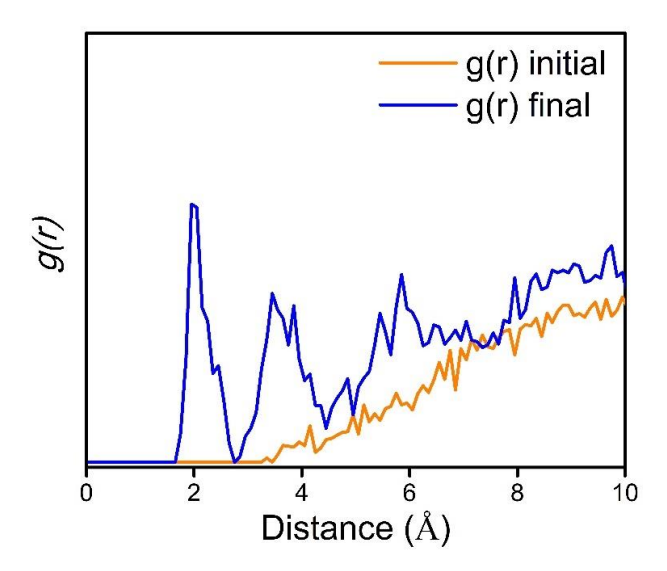


Figure S9 *RDF* calculations of the initial and final 0.25 ps of the MXene/Water/NaAsc simulations.

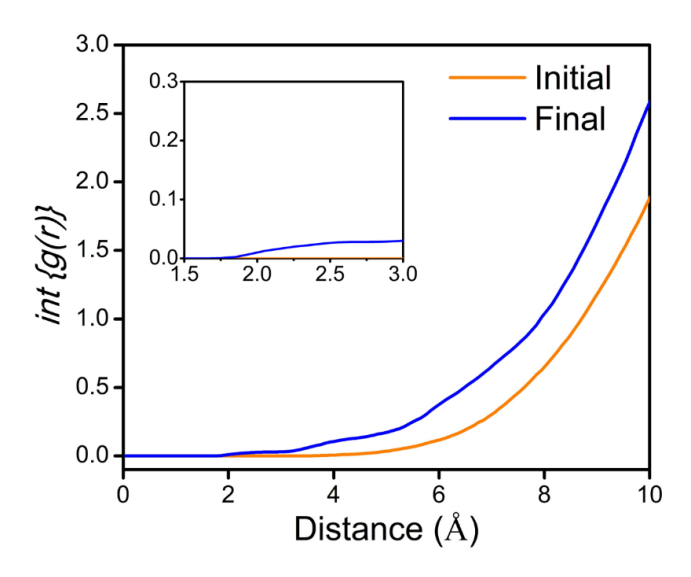


Figure S10 Number integral of g(r) for Na-O bond at the initial and final 0.25 ps of the MXene/Water/NaAsc simulations.

EDS measurements after washing away cations

Here, we assess whether sodium cations can be removed from MXenes in the buckypaper by repeated washing. Stored MXene colloid was vacuum filtered to make films. After that, different amounts of distilled water were used to rinse the film by vacuum filtration. The MXene films were then dried under vacuum for 12 hours. The sodium residues in the dried MXene films were monitored by Energy-dispersive X-ray spectroscopy (EDS). Since all the titanium detected on the film comes from MXene, the weight and atomic ratios between Na and Ti (Na: Ti) are a reasonable metric to quantify the sodium content. A sample made by freeze drying the NaAsc-stabilized MXene colloid was chosen as a reference since no sodium is removed in that case. Table S5 reveals that sodium can be nearly removed in full after adequate washing process. After being washed by 100 ml water, the sodium content became low, so it may be barely detected (the standard deviation is close to the obtained the weight percentage itself, which we did not report it in detail). We believed that most of the sodium and excess ascorbate groups left the MXene samples during the filtration process. This suggests a weak interaction between sodium cation and individual MXene nanosheets, which is consistent with the simulation results. In addition, Ren et al. reported that sodium cations carrying a relatively small hydration radii have a fast permeation rate through the 2D nanochannels and layer space in MXene films. In conclusion, the interaction between sodium cations and MXene nanosheets is limited. The strong adsorption and intercalation will not happen in our case for individual nanosheets when the concentration of NaAsc is kept low. In contrast, adequate ascorbate groups will interact with and stabilize the MXene nanosheets. Note that we add NaAsc in excess amount.

Table S5 Sodium to titanium ratios, which are measured by Energy-dispersive X-ray spectroscopy (EDS), decreases with the increasing of the washing stages for the NaAsc treated MXenes.

	Freeze dried	Vacuum filtration	Vacuum filtration	Vacuum filtration
	with no	with limited wash	with moderate wash	with adequate wash
	wash	(2 ml H ₂ O)	(50 ml H ₂ O)	(100 ml H ₂ O)
Na: Ti (wt %)	1:2	1:27	1:103	1:163
N. T. (+ 0 ()	1.1	1.12	1.50	1.00
Na: Ti (at %)	1:1	1:13	1:50	1:80

References

1.	Osti, N.C., et al., Effect of Metal Ion Intercalation on the Structure of MXene and Water Dynamics
	on its Internal Surfaces. Acs Applied Materials & Interfaces, 2016. 8(14): p. 8859-8863.